ACS OMEGA

http://pubs.acs.org/journal/acsodf

Article

Strategy of Integrating Ultraviolet Absorption and Antimicrobial Activity in a Single Molecule: DFT Calculation and Experiment

Mingli Shan*

Cite This: *ACS Omega* 2022, 7, 41575−41580

Read Online

ACCESS | Metrics & More | Article Recommendations

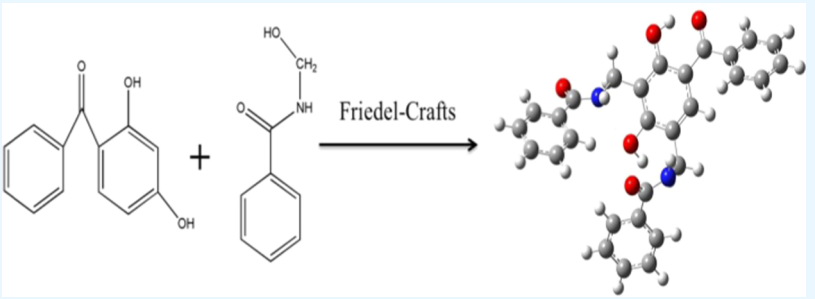

ABSTRACT: In the present study, (3,5-benzamide-2,4-dihydroxyphenyl)(phenyl) methanone (UV-CB) was synthesized and investigated as an ultraviolet (UV) absorber and a bacteriostatic agent. The optimized geometry, energy levels, charges, and UV electronic absorption bands of UV-CB in the singlet were calculated by density functional theory (DFT) calculations. The quantum chemical method was used to investigate the geometry and natural bond orbital (NBO) parameters. And the computational studies indicated that the intramolecular hydrogen bond (IMHB) was formed between the 2,4-dihydroxybenzophenone (UV-C) group and the *N*-(hydroxymethyl)benzamide (NBA) group, which was beneficial to the stability after the combination. The results of the minimum inhibitory concentration (MIC) and minimum bactericidal concentration (MBC) tests illustrated that UV-CB is a promising antibacterial agent. The successful synthesis of UV-CB with anti-UV performance and antibacterial ability evidences that DFT calculation is an available approach to design and analyze novel compounds.

1. INTRODUCTION

Polymer materials are widely applied in various industrial fields due to their high stability, easy application, and low manufacturing costs. However, polymer materials are vulnerable to ultraviolet (UV), which results in reduced physical and chemical properties.[1−3] Polymer photodegradation limited the intrinsic stability and service life of polymers. The application of UV absorbers solves the UV aging problem of polymer materials.[4−6] Benzotriazoles and benzophenones are dominant commercial UV absorbers, which have been used to protect polymer materials from UV aging for decades. In addition to the excellent ultraviolet absorption, high photostability is another key property of UV absorbers. As a classical UV absorber, UV-C has been widely used for decades; however, its photostability is unsatisfactory.[7,8] As such, the classical UV absorbers must be dramatically improved for future applications.[9] The previous reports show that an effective approach to increase photostability is to introduce more intramolecular hydrogen bonds, which can lead to the conversion of the absorbed ultraviolet energy into heat without chemical damage, just like benzotriazoles and benzophenones.[10] Therefore, much effort has been devoted to synthesizing novel UV absorbers with highly efficient ultraviolet absorption and more IMHBs by combining different functional groups in one molecule.[11]

In the natural environment, polymer materials are degraded by both physical and biological factors.[12] Microbiological degradation is also a non-negligible adverse factor of polymer materials because polymer materials are potential sources of carbon and nitrogen for heterotrophic microorganisms.[13−15] Polymer materials are degraded to metabolic products (H_2O, CO_2, and CH_4) by the enzymatic reaction of microorganisms, leading to changes in their structure and performance.[16−18] To protect against microbiological degradation, antibacterial agents are used to restrain the microorganisms as functional additives.[19,20] Hence, we envisioned that to combine antibacterial and anti-UV abilities in one single species using a facile one-step method might be a meaningful strategy.

Received: August 24, 2022
Accepted: October 20, 2022
Published: November 1, 2022

https://doi.org/10.1021/acsomega.2c05438
ACS Omega 2022, 7, 41575−41580

Scheme 1. Synthetic Route of UV-CB

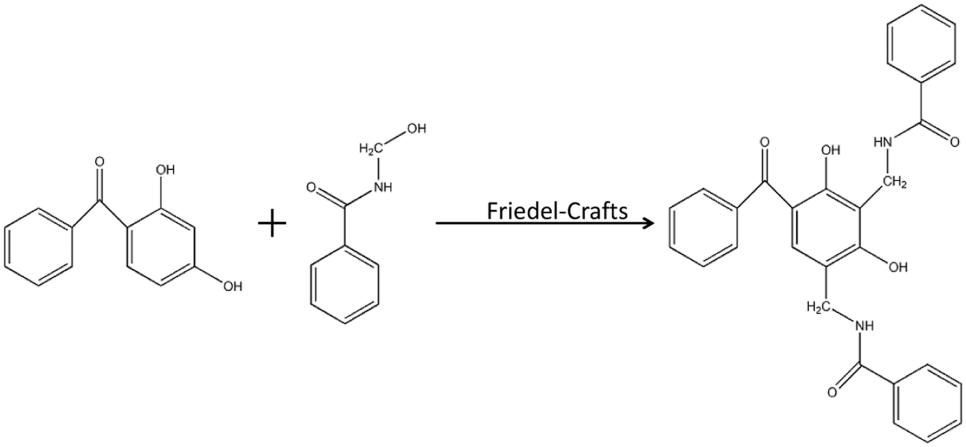

More recently, environmentally friendly natural-like antibacterial agents have received extensive attention, such as capsaicin derivatives.[21] To construct a new UV absorber with improved photostability based on UV-C, the NBA groups were introduced under the guidance of DFT calculations in this work. After the combination, capsaicin moiety functional groups were observed between the UV-C and NBA parts, indicating that the newly synthesized compound is a promising antibacterial agent.[22]

Herein, a novel IMHB-rich polymer additive with anti-UV performance and antibacterial ability has been successfully designed and synthesized using UV-C and NBA. The electron distribution and the active site of UV-C and NBA were predicted by DFT calculation. The anti-UV performance of the polymer additive was calculated via quantum chemical calculation. The anti-UV performance of the polymer additive was measured by the UV absorption spectrum. The antibacterial ability of the polymer additive was investigated by an antimicrobial test. The antimicrobial test was utilized to investigate the antibacterial ability of the polymer additive. The calculations showed a good correlation between the computational studies and the experimental data, indicating that DFT calculation is an available strategy in the design and analysis of novel compounds.

2. MATERIALS AND METHODS

2.1. Materials and Reagents. UV-C, NBA, $AlCl_3$, acetone, concentrated hydrochloric acid, and anhydrous ethanol were purchased from Guoyao (China). Agar-based solid medium and liquid medium were obtained from Bailingwei (China). *Escherichia coli*, *Staphylococcus aureus*, and culture medium were kindly provided by the Ocean University of China.

2.2. Characterizations. The UV absorption spectra of the synthetic UV absorber were recorded on a Lambda 900 UV−vis spectrometer and using dimethyl formamide (DMF) as solvent. Infrared spectra were recorded on a Bruker IFS-113 spectrometer (KBr pellets). ^{13}C and ^{1}H NMR spectroscopies were performed on a Bruker DRX-250 spectrometer in dimethyl sulfoxide solution. ESI mass spectra were recorded on a TQ-8030 mass spectrometer. Elemental analysis was recorded on a 3V-EDX8600 Elementar. The bacteriostatic properties were investigated with the MIC and MBC of *E. coli* and *S. aureus*.

2.3. Synthesis of UV-CB. The synthetic route of UV-CB is shown in Scheme 1. $AlCl_3$ (0.001 mol) was dissolved in acetone (30 mL) under vigorous agitation, and then UV-C (0.01 mol) and NBA (0.02 mol) were added, and the mixture was stirred for 50 h at 40 °C. On completion, the reaction was cooled to ambient temperature. The precipitate was isolated by filtration, washed with diluted hydrochloric acid, and dried in vacuum. Immediately thereafter, the obtained powder was further purified by recrystallization from ethanol (15 mL) and afforded 3.98 g (yield 83%) of UV-CB as a white solid. m.p. 256−257 °C; FTIR (KBr)/cm^{-1}: 3365, 32 784(OH), 3081(NH), 1656, 1623(C═O); ^{1}H NMR (600 MHz, DMSO-d_6)/ppm: δ 13.13 (s, 1H, O−H), 11.95 (s, 1H, O−H), 9.64 (t, J = 6.0 Hz, 1H, N−H), 8.97 (t, J = 6.0 Hz, 1H, N−H), 7.96 (d, J = 7.2 Hz, 2H, Ar−H), 7.78 (d, J = 7.2 Hz, 2H, Ar−H), 7.58 (d, J = 6.6 Hz, 3H, Ar−H), 7.54 (d, J = 1.2 Hz, 2H, Ar−H), 7.50 (t, J = 7.8 Hz, 2H, Ar−H), 7.45 (d, J = 6.0 Hz, 3H, Ar−H), 7.41 (d, J = 8.1 Hz, 2H, Ar−H), 4.55 (d, J = 5.4 Hz, 2H, $-CH_2-$), 4.37 (d, J = 6.0 Hz, 2H, $-CH_2-$); ^{13}C NMR (150 MHz, DMSO-d_6): 199.8, 169.6, 167.4, 163.2, 162.1, 138.0, 134.5, 133.3, 132.9, 132.5, 132.0, 131.8, 129.1, 128.9, 128.8, 128.7, 128.1, 127.6, 118.9, 112.9, 111.6, 38.4, 33.2; mass (ESI) found m/z: 481.1775; element analysis: found (%): C, 72.50, H, 5.01, N, 5.86; calcd (%): C, 72.45, H, 5.08, N, 5.82.

2.4. Calculations. In this work, by allowing the relaxation of all of the parameters, the calculation has been found to converge to an optimized geometry at the M062X/6-311G(d) level, as revealed by the absence of imaginary values in the calculated wavenumbers of all of the vibrational modes. The electronic transition energies, electronic transition orbital, and molecular electrostatic potential (MEP) were calculated by the M062X/6-311++G(d,p) method.[23] The cluster model and the self-consistent isodensity polarizable continuum model (SCI-PCM) were used to explain the UV absorption spectra of UV-CB in DMF solution at the M062X/6-311++G(d,p) level. For the weak interaction energy analysis, second-order Moller−Plesset theory (MP2) is more reliable than density functional theory. In this work, MP2 was used to investigate the IMHB interaction of UV-CB based on the M062X/6-311G(d) level optimized structure.[24−26] The calculations in this work were implemented in the Gaussian09 package.

2.5. Antimicrobial Activity Test. A solution of the UV-CB in acetone (1.0 mL, 6.0 mg/mL) was mixed with liquid medium (2.0 mL). Then, the mixture was diluted by the serial double dilution method to obtain gradient concentrations of experimental solution (2.0, 1.0, 0.5, 0.25, 0.125, 0.0625, 0.0313, 0.0157 mg/mL). The bacterial suspension (200 μL) was added to the experimental solution with 24 h of culture at 37 °C. The bacterial solution with UV-C was used to carry out control

https://doi.org/10.1021/acsomega.2c05438
ACS Omega 2022, 7, 41575−41580

experiments. The lowest concentrations of UV-CB that achieved a 99% decrease on the plates after 48 h of incubation at 37 °C were recorded as the minimum bactericidal concentrations (MBCs). The MICs and MBCs were determined from the curve of concentration versus OD600.[27,28]

3. RESULTS AND DISCUSSION

3.1. Theory-Guided Design. The Friedel−Crafts reaction is an effective method to incorporate functional groups with aromatic rings. According to Markovnikov's rule, the electron-rich atoms are most likely to be attacked by electrophilic substituents.[29,30] In this fashion, analyzing the electron distribution of the substituted aromatic compound is a promising method to predict the molecular structure. Figure 1

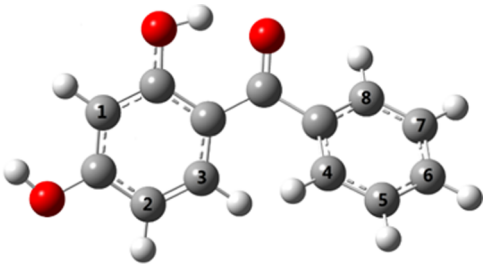

Figure 1. S_0-optimized structure of UV-C at the M062X/6-311++G(d) level (red: O atom, white: H atom, gray: C atom).

shows the optimized geometry of UV-C. The corresponding electron distribution calculated by NBO is summarized in Table 1. It is obvious that the electron-rich atoms C_1 and C_2 have a similar natural charge and natural population. As a consequence, C_1 and C_2 positions are readily attacked by substituents to form bis-substituted compounds.

The optimized structure of the UV-CB has two IMHBs, as shown in Figure 2, in which one is in the UV-C group (bond length: 1.588 Å) and another is formed by UV-C and NBA groups (bond length: 1.655 Å). As an effective method of spectral data analysis, quantum chemistry calculations are in good agreement with the experimental spectra.[31] The cluster model and the self-consistent isodensity polarizable continuum model were used to calculate the UV−vis absorption spectrum of UV-CB in DMF, as shown in Figure 3; the obtained results reveal that the UV-CB structure has two strong UV absorption bands with the maximum molar absorption coefficient of 12950 and 15480 L/mol·cm. Therefore, the quantum chemistry calculations can predict that the new synthesized UV-CB is an effective ultraviolet absorber.

3.2. Absorption Spectrum. The pivotal calculation results of NBO are listed in Table 2. By contrast, oscillator strengths (f) of 0.2256 and 0.2969 with the transition orbitals of 126 → 127 and 125 → 127 are plainly stronger, contributing to the two salient absorption bands located at 335 and 299 nm. As shown in Table 2 and Figure 4, the electronic transition bands of the UV-CB calculated by DFT show unexceptionable consistency with the experimental spectra.

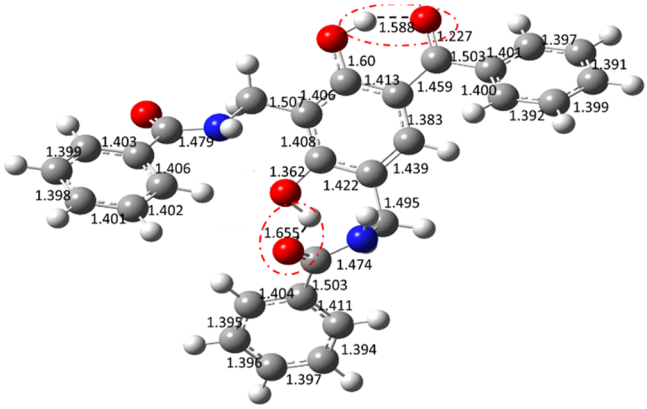

Figure 2. S_0-optimized structure of UV-CB at the M062X/6-311++G(d) level. Bond length in Å, red: O atom, blue: N atom, white: H atom, gray: C atom.

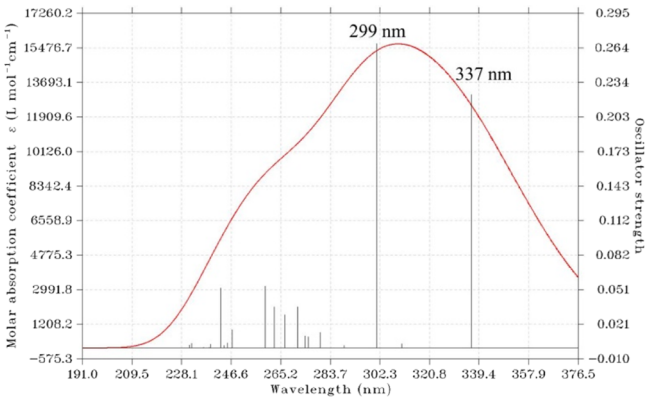

Figure 3. Absorption spectra of UV-CB at the M062X/6-311++G(d,p) level.

Figure 5 shows the orbitals (125, 126, and 127) associated with the $S_0 \rightarrow S_1$ and $S_0 \rightarrow S_4$ electronic transitions, indicating that orbitals 125 (HOMO − 1), 126 (HOMO), and 127 (LUMO) are π orbitals. For orbital 125, the electronic clouds are localized at one of the NBA groups, the electronic clouds of orbital 126 are localized at the UV-C group and one of the NBA groups, and the electronic clouds of orbital 127 are distributed only at the UV-C group. According to the calculation results, the distinct UV absorption peaks at 344 nm and 297 nm belong to the $\pi \rightarrow \pi^*$ transition.[11] Obviously, the S0 → S1 (126 → 127) and S0 → S4 (125 → 127) transitions are the processes of electron cloud transfer from NBA groups to the UV-C group. As shown in Figure 5, although the NBA groups contribute to the electronic transitions, the limited involvement results in the negligible distinction between the UV absorption spectra of UV-C and UV-CB.

3.3. IMHB Interaction and Molecular Electrostatic Potential. The parameters calculated based on Figure 2 illustrate that there are two IMHBs in the UV-CB, which can be verified by NBO calculations, as shown in Table 3. Therefore, the strength of the IMHBs can be determined by the amount of

Table 1. Natural Charge and Natural Population of UV-C Calculated from M062X/6-311++G(d)[a]

atom	C_1	C_2	C_3	C_4	C_5	C_6	C_7	C_8
natural charge (e)	−0.383	−0.323	−0.176	−0.221	−0.232	−0.221	−0.235	−0.192

[a]The number of carbon atoms is labeled in Figure 1.

https://doi.org/10.1021/acsomega.2c05438
ACS Omega 2022, 7, 41575−41580

Table 2. Transition States, Character, Transition Orbitals, Electronic Transition Energies, and Oscillator Strengths (f) for UV-CB Calculated from M062X/6-311++G(d,p)

			transition energy (eV)		
transition state	character	transition orbitals	calc.	expt.	oscillator strength (f)
$S_0 \rightarrow S_1$	$^1(\pi, \pi^*)$	126 → 127 (0.71)	4.23 (337 nm)	344 nm	0.2256
$S_0 \rightarrow S_2$	$^1(\pi, \pi^*)$	126 → 128 (0.49)	4.01 (314 nm)		0.0019
$S_0 \rightarrow S_3$	$^1(\pi, \pi^*)$	126 → 128 (0.41)	3.99 (312 nm)		0.0005
$S_0 \rightarrow S_4$	$^1(\pi, \pi^*)$	125 → 127 (0.66)	4.61 (299 nm)	297 nm	0.2969
$S_0 \rightarrow S_5$	$^1(\pi, \pi^*)$	125 → 128 (0.73)	4.86 (289 nm)		0.0537
$S_0 \rightarrow S_6$	$^1(\pi, \pi^*)$	126 → 129 (0.45)	4.89 (283 nm)		0.0069
$S_0 \rightarrow S_7$	$^1(\pi, \pi^*)$	124 → 127 (0.61)	4.92 (281 nm)		0.0199

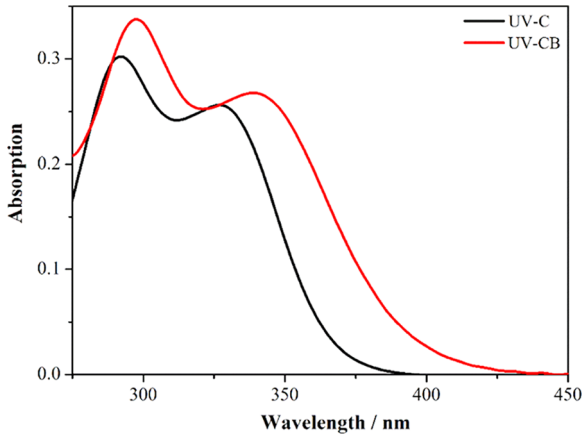

Figure 4. UV−vis absorption spectra of UV-C and UV-CB in 2×10^{-5} M DMF.

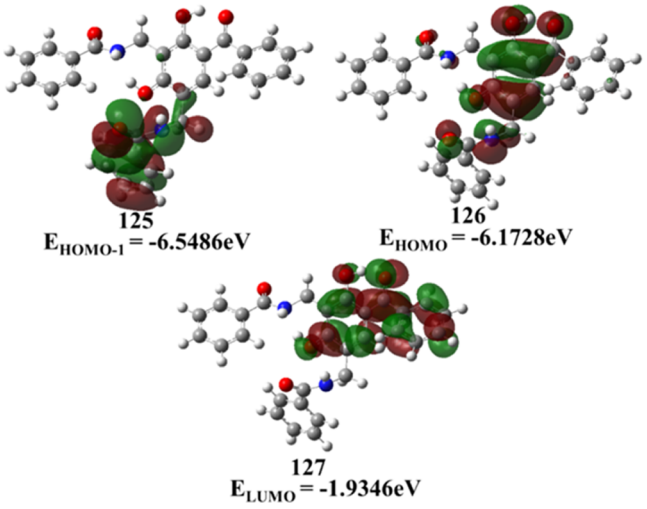

Figure 5. Molecular orbitals (125, 126, and 127) for the strong absorption bands of UV-CB above the 275 nm region at the M062X/6-311++G(d,p) level.

charge transfer. The values of NBO second-order interaction energies $\Delta E_{ij}^{(2)}$ are a significant indicator to estimate the interaction strength of IMHBs.[26] $\Delta E_{ij}^{(2)}$ is calculated as

$$\Delta E_{ij}^{(2)} = \frac{|\langle \varnothing_i | \hat{F} | \varnothing_j^2 \rangle|}{(\varepsilon_i - \varepsilon_j)}$$

NBO calculations indicate that the sum $\Delta E_{ij}^{(2)}$ of O−H···O generated by the UV-C part and the NBA part is 30.19 kcal/mol, while that of O−H···O in the UV-C part is 43.69 kcal/mol, indicating that IMHB in the UV-C part is much stronger.

Molecular electrostatic potential (MEP) closely correlates with electron density distribution and is a very useful descriptor for revealing preferential sites of electrostatically dominated noncovalent interactions. The MEP plot provides a clear description of the electronic nature of the UV-CB, as shown in Figure 6, while the blue and red regions correspond to the

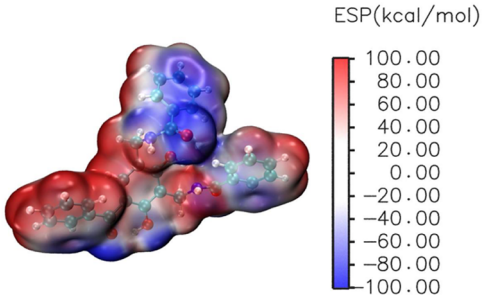

Figure 6. Molecular electrostatic potential of UV-CB at the M062X/6-311++G(d,p) level.

most negative and positive MEP on the UV-CB surface, respectively. Additionally, in Figure 6, the significant surface local maxima and minima of MEP are represented as orange and cyan, respectively. It can be seen that the oxygen atom belonging to OH leads to a MEP minima, while the global surface maximum is found around the NH group.

3.4. Antimicrobial Activity. *E. coli* and *S. aureus* were used as the model bacteria to evaluate the antimicrobial activity of

Table 3. Structural Parameters and NBO Analysis for IMHB in UV-CB at the M062X/6-311++G(d,p) Level

				NBO[a]		
IMHB	r(O−H), Å	r(O−H···O), Å	∠(O−H···O), deg	ϕ_i	ϕ_j	$\Delta E_{ij}^{(2)}$
O−H···O[b]	1.004	2.517	141.7	O	σ^*_{O-H}	30.19
O−H···O[c]	0.997	2.661	148.6	O	σ^*_{O-H}	41.69

[a]NBO donor orbitals ϕ_i; acceptor orbitals ϕ_i, and their corresponding second-order interaction energies $\Delta E_{ij}^{(2)}$ in kcal/mol. [b]O−H···O formed between the UV-C group and one of the NBA groups. [c]O−H···O in the UV-C group.

https://doi.org/10.1021/acsomega.2c05438
ACS Omega 2022, 7, 41575−41580

UV-CB, while UV-C was tested as a reference. The MIC and MBC values, listed in Table 4, show that their activities against

Table 4. Antimicrobial Activities of UV-C and UV-CB

	E. coli bacteria		*S. aureus*	
compound	MIC (mg/L)	MBC (mg/L)	MIC (mg/L)	MBC (mg/L)
UV-C	1.0		1.0	
UV-CB	0.0313	0.0607	0.0157	0.0336

tested microorganisms are different. Both the MIC and MBC values of UV-CB for *S. aureus* decreased by nearly 50% compared with *E. coli*, indicating that UV-CB was more active against *S. aureus*. UV-CB exhibited remarkable antimicrobial performance compared with UV-C, indicating that antimicrobial functional groups were newly formed after the combination. These results afford the ground information for the potential use of UV-CB as an efficient bacteriostatic agent with favorable MIC and MBC values.

4. CONCLUSIONS

In summary, a novel UV absorber with antimicrobial ability based on quantum chemistry has been successfully fabricated. After rigorous calculation and analysis, a conclusion is drawn that the maximum absorption peaks of UV-CB are derived from the electronic transition bands of $S_0 \rightarrow S_1$ and $S_0 \rightarrow S_4$. The UV absorption spectrum calculated by TD-DFT manifests excellent agreement with the experimental data. The results of the present study demonstrate the UV-CB with both high antimicrobial activity and remarkable UV-absorbing ability, confirming that the quantum chemistry calculation can provide guidance for the synthesis of new compounds.

AUTHOR INFORMATION

Corresponding Author

Mingli Shan − *Zibo Vocational Institute, Zibo 255000, China; Key Laboratory of Marine Chemistry Theory and Technology, Ministry of Education, Ocean University of China, Qingdao 266100, China;* orcid.org/0000-0002-8021-7204; Phone: (86) 532-66782533; Email: shanmingli1987@163.com

Complete contact information is available at: https://pubs.acs.org/10.1021/acsomega.2c05438

Author Contributions

M.S. performed all of the works in the investigation, calculation, and writing—review and editing.

Notes

The author declares no competing financial interest.

ACKNOWLEDGMENTS

This project was supported by the Joint Funds of the National Natural Science Foundation of China (Grant No. U1706225) and the Fundamental Research Funds for the Central Universities (201562026 and 201762029).

REFERENCES

(1) Saadat-Monfared, A.; Mohseni, M. Polyurethane nanocomposite films containing nano-cerium oxide as UV absorber; Part 2: Structural and mechanical studies upon UV exposure. *Colloids Surf., A* **2014**, *441*, 752−757.

(2) Gao, Y.; Gu, Y.; Wei, Y. Determination of polymer additives-antioxidants and ultraviolet (uv) absorbers by high-performance liquid chromatography coupled with uv photodiode array detection in food simulants. *J. Agric. Food Chem.* **2011**, *59*, 12982−12989.

(3) Zhao, Y.; Xu, Z.; Wang, X.; Tong, L. Superhydrophobic and UV-blocking cotton fabrics prepared by layer-by-layer assembly of organic UV absorber intercalated layered double hydroxides. *Surf. Sci.* **2013**, *286*, 364−370.

(4) Grüneberger, F.; Künniger, T.; Huch, A.; Zimmermann, T.; Arnold, M. Nanofibrillated cellulose in wood coatings: Dispersion and stabilization of ZnO as UV absorber. *Prog. Org. Coat.* **2015**, *87*, 112−121.

(5) Coelho, C.; Thomas, S.; Fabrice, L.; Vincent, V. Inorganic-Organic Hybrid Materials Based on Amino Acid Modified Hydrotalcites Used as UV-Absorber Fillers for Polybutylene Succinate. *Eur. J. Inorg. Chem.* **2015**, *2012*, 5252−5258.

(6) Queant, C.; Blanchet, P.; Landry, V.; Schorr, D. Effect of adding uv absorbers embedded in carbonate calcium templates covered with light responsive polymer into a clear wood coating. *Coatings* **2018**, *8*, 265−279.

(7) Westlake, J. F.; Johnson, M. Diffusion of stabilizers in polymers. I. 2; 4-dihydroxybenzophenone in polyolefins. *J. Appl. Polym. Sci.* **1975**, *19*, 319−334.

(8) Inoue, K.; Takahata, H.; Tanigaki, T. Novel UV absorbers prepared from 2; 4-dihydroxybenzophenone and hexachlorocyclotriphosphazene. *J. Appl. Polym. Sci.* **1993**, *50*, 1857−1862.

(9) Li, S.; Shen, Y.; Xiao, M.; Liu, D.; Fa, L.; Wu, K. Intercalation of 2; 4-dihydroxybenzophenone-5-sulfonate anion into Zn/Al layered double hydroxides for UV absorption properties. *J. Ind. Eng. Chem.* **2014**, *20*, 1280−1284.

(10) Pei, K.; Cui, Z.; Chen, W. An adduct of Cl-substituted benzotriazole and hydroxy benzophenone as a novel UVA/UVB absorber: Theory-guided design; synthesis; and calculations. *J. Mol. Struct.* **2013**, *1032*, 100−104.

(11) Shan, M.; Liu, Y.; Xia, S.; Tang, Q.; Yu, L. A strategy of integrating ultraviolet absorption and crosslinking in a single molecule: DFT calculation and experimental. *J. Mol. Struct.* **2016**, *1107*, 249−253.

(12) Gu, J. Microbiological deterioration and degradation of synthetic polymeric materials: recent research advances. *Biodegradation* **2003**, *52*, 69−91.

(13) Hefni, Y.-K. Hydrophobic Zinc Oxide Nanocomposites for Consolidation and Protection of Quartzite Sculptures: A Case Study. *J. Nano Res.* **2020**, *63*, 64−75.

(14) Gu, J.-D.; Ford, T.; Thorp, K.; Mitchell, R. Microbial growth on fiber reinforced composite materials. *Int. Biodeterior. Biodegrad.* **1996**, *37*, 197−204.

(15) Gu, J.; Gu, J. Methods Currently Used in Testing Microbiological Degradation and Deterioration of a Wide Range of Polymeric Materials with Various Degree of Degradability: A Review. *Polym. Environ.* **2005**, *13*, 65−74.

(16) Liang, D.-W.; Zhang, T.; Fang, H. Denitrifying degradation of dimethy phthalate. *Appl. Microbiol. Biotechnol.* **2007**, *74*, 221−229.

(17) Gu, J.-D.; Kigawa, R.; Sato, Y.; Katayama, Y. Addressing the microbiological problems of cultural property and archive documents after earthquake and tsunami. *Int. Biodeterior. Biodegrad.* **2013**, *85*, 345−346.

(18) Lu, B.; Lin, Y.; Tsai, Y.; Girman, S.; Adamus, G.; Jones, M. K.; Shelley, B.; Svendsen, C. N.; Wang, S. A Subsequent Human Neural Progenitor Transplant into the Degenerate Retina Does Not Compromise Initial Graft Survival or Therapeutic Efficacy. *Transl. Vis. Sci. Technol.* **2015**, *4*, 7−21.

(19) Jendrossek, D.; Knoke, I.; Habibian, R. B.; Steinbüchel, A.; Schlegel, H. G. Degradation of poly(3-hydroxybutyrate), PHB, by bacteria and purification of a novel PHB depolymerase from Comamonas sp. *J. Environ. Polym. Degrad.* **1993**, *1*, 53−63.

(20) Gu, J.-D.; Eberiel, D.; Mccarthy, S.; Gross, R. Cellulose acetate biodegradability upon exposure to simulated aerobic composting and anaerobic bioreactor environments. *J. Environ. Polym. Degrad.* **1993**, *1*, 143−153.

https://doi.org/10.1021/acsomega.2c05438
ACS Omega 2022, 7, 41575−41580

(21) Wang, Z.-C.; Wei, B.; Pei, F.; Yang, T.; Tang, J.; Yang, S.; Yang, F.; et al. Capsaicin derivatives with nitrothiophene substituents: Design; synthesis and antibacterial activity against multidrug-resistant *S. aureus*. *Eur. J. Med. Chem.* **2020**, *198*, No. 112352.
(22) Zhou, J.; Zhang, X.; Yan, Y.; Hu, J.; Wang, H.; Cai, Y.; Qu, J. Preparation and characterization of a novel antibacterial acrylate polymer composite modified with capsaicin. *Chin. J. Chem. Eng.* **2019**, *27*, 3043−3052.
(23) Paul, S.; Mallick, A.; Majumdar, T. Computational Study on the Ion Interaction of Ellipticine: A Theoretical Approach towards Selecting the Appropriate Anion. *Chem. Phys. Lett.* **2015**, *634*, 29−36.
(24) Takahashi, N.; Shinno, T.; Tachikawa, M.; Yuzawa, T.; Takahashi, H. Time-resolved resonance Raman; time-resolved UV−visible absorption and DFT calculation study on photo-oxidation of the reduced form of nicotinamide adenine dinucleotide. *J. Raman Spectrosc.* **2006**, *37*, 283−290.
(25) Almandoz, M.-K.; Sancho, M.-I.; Duchowicz, P.-R.; Blanco, S.-E. UV-Vis spectroscopic study and DFT calculation on the solvent effect of trimethoprim in neat solvents and aqueous mixtures. *Spectrochim. Acta, Part A* **2014**, *129*, 52−60.
(26) Yang, J.-W.; Choi, J.-K.; Kim, M.-C.; Kim, H. A study of UV−vis spectroscopic and DFT calculation of the UV absorber in different solvent. *Prog. Org. Coat.* **2019**, *135*, 168−175.
(27) Eloff, N.-J. The presence of antibacterial compounds in *Anthocleista grandiflora* (Loganiaceae). *S. Afr. J. Bot.* **1998**, *64*, 209−212.
(28) Wiegand, I.; Kai, K.; Hancock, R. Agar and broth dilution methods to determine the minimal inhibitory concentration (MIC) of antimicrobial substances. *Nat. Protoc.* **2008**, *3*, 163−175.
(29) Kumar, A.; Kumar, M.; Gupta, M.-K. An efficient organo-catalyzed multicomponent synthesis of diarylmethanes via Mannich type Friedel−Crafts reaction. *Tetrahedron Lett.* **2009**, *50*, 7024−7027.
(30) Liu, W.; Zhao, C.; Zhou, Y.; Xu, X. Modeling of Vapor-Liquid Equilibrium for Electrolyte Solutions Based on COSMO-RS Interaction. *J. Chem.* **2022**, *2022*, No. 9070055.
(31) Karabacak, M.; Cinar, Z.; Kurt, M.; Sudha, S.; Sundaraganesan, N. FT-IR; FT-Raman; NMR and UV−vis spectra; vibrational assignments and DFT calculations of 4-butyl benzoic acid. *Spectrochim. Acta, Part A* **2012**, *85*, 179−189.

https://doi.org/10.1021/acsomega.2c05438
ACS Omega 2022, 7, 41575−41580